# ANALYSIS OF COMPOSITE HYDROGEN STORAGE CYLINDERS UNDER TRANSIENT THERMAL LOADS

**Hu, J.[1], Sundararaman, S.[2], Chandrashekhara, K.[3]* and Chernicoff, W.[4]**

**[1, 2, 3] Department of Mechanical and Aerospace Engineering, University of Missouri-Rolla Rolla, MO 65409**
**[4] US Department of Transportation, Washington, DC 20590**

## ABSTRACT

In order to ensure safe operation of hydrogen storage cylinders under adverse conditions, one should be able to predict the extremities under which these cylinders are capable of operating without failing catastrophically. It is therefore necessary to develop a comprehensive model which can predict the behavior and failure of composite storage cylinders when subjected to various types of loading conditions and operating environments. In the present work, a finite element model has been developed to analyze composite hydrogen storage cylinders subjected to transient localized thermal loads and internal pressure. The composite cylinder consists of an aluminum liner that serves as a hydrogen gas permeation barrier. A filament-wound, carbon/epoxy composite laminate placed over the liner provides the desired load bearing capacity. A glass/epoxy layer or other material is placed over the carbon/epoxy laminate to provide damage resistance for the carbon/epoxy laminates. A doubly curved composite shell element accounting for transverse shear deformation and geometric nonlinearity is used. A temperature dependent material model has been developed and implemented in ABAQUS using user subroutine. A failure model based on Hashin's failure theory is used to predict the various types of failure in the cylinder. A progressive damage model has also been implemented to account for reduction in modulus due to failure. A sublaminate model has been developed to save computational time and reduce the complications in the analysis. A numerical study is conducted to analyze a typical hydrogen storage cylinder and possible failure trends due to localized thermal loading and internal pressure is presented.

KEYWORDS: composite cylinder, transient thermal loads, finite element analysis, progressive damage

*Author for Correspondence: K. Chandrashekhara, Professor, Department of Mechanical and Aerospace Engineering, University of Missouri-Rolla, MO 65409. E-mail: chandra@umr.edu, Phone: 573-341-4587, Fax: 573-341-6899.

## 1.0 INTRODUCTION

Composite storage cylinders offer light weight, corrosion resistance, dimensional stability and can store gas at higher pressures. However, the current design methodology cannot yet guarantee their safe operation [1]. Typically, a composite high-pressure cylinder is made with a high molecular weight polymer or aluminum liner that serves as a hydrogen gas permeation barrier. A filament-wound, carbon/epoxy composite laminate over-wrapped outside of the liner provides the desired pressure load bearing capacity. Composite hydrogen storage cylinders are usually under a pressure of 5000 psi or higher and are also subjected to external temperature variations. As composite materials in general are sensitive to combined thermo-mechanical loads, it is necessary to study the effect of this combined loading for safe design and operation.

Studies have been conducted on composite hydrogen storage cylinders subjected to thermal loads and combined thermo-mechanical loads. Parnas and Katirici [2] developed an analytical procedure to design and predict the behavior of composite hydrogen storage cylinder taking into account thermal and moisture effects. Akcay and Kaynak [3] analyzed a glass/epoxy multilayered composite cylinder under both plane-strain and closed-end conditions. Sayman [4] expanded this work by accounting for uniform temperature distribution and moisture effects. Some research has also been conducted on analysis of composite cylinders subjected to transient thermal loads but most of it has been limited to analytical work. Yee and Moon [5] developed a closed form analytical solution for transient plane thermal stress analysis of linear elastic, homogeneously orthotropic hollow cylinders subjected to an arbitrary temperature distribution. Lee et al. [6] developed a model to analyze thermal stresses in multilayered hollow cylinder. Laplace transforms and finite difference method was used for the analysis. Lu et al. [7] developed an analytical solution for transient heat conduction in multi-dimensional composite cylinder slab. Jacquemin and Vautri [8] developed an analytical solution for calculation of transient thermoelastic stresses in thick walled composite anisotropic pipes. However, no studies have been conducted on analysis of hydrogen storage cylinders subjected to localized thermal loading and pressure.

In the present study, a finite element model has been developed to analyze composite hydrogen storage cylinders subjected to transient localized thermal loads and internal pressure. A laminated shell theory [9] accounting for out-of-plane shear strains and geometric nonlinearity is used for the analysis. A sublaminate model has been adopted to reduce computational time. The variation of material properties with temperature is significant for most composites and cannot be ignored. A temperature dependent material model has been developed and implemented in commercial finite element code ABAQUS, using user subroutines. A failure model based on Hashin's failure theory has been implemented in ABAQUS. To account for material property reduction due to composite failure, a progressive damage model has also been incorporated.

## 2.0 MODELING

A strong sequentially coupled thermal-stress approach is implemented in predicting the behavior of composite hydrogen cylinder subjected to transient thermal loading and internal pressure. At each increment, the temperature profile is obtained using the thermal model. The temperature field is then imported to the mechanical model with material damage information from previous increment. The thermal and mechanical models have to be solved sequentially in each increment. A doubly curved shell theory is used for modeling laminated composite cylinder. The theory considers both out of plane shear deformations and geometric nonlinearity and also accounts for the nonlinear variation of temperature through the shell thickness. As the wall consists of large number of laminae, modeling each lamina will cause extraordinary computational cost, especially when thermal and damage models are also

incorporated. Hence, a homogenization technique is used to smear the angle-ply helical layers to sublaminates.

### 2.1 Doubly Curved Shell Thermal-stress Model

A multilayered doubly curved shell is shown in Figure 1. The curved coordinated system $\{\xi_1, \ \xi_2, \ \zeta\}$ is used in space description. The coordinates $\xi_1$ and $\xi_2$ specify the position on the middle surface, while $\zeta$ measures the distance, along the outward normal, from the mid-surface to an arbitrary point on the shell. The displacement field can be written as [10]:

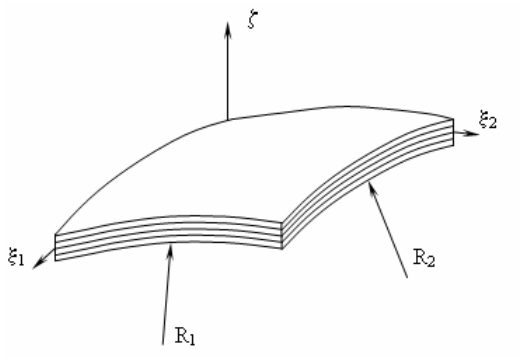


Figure 1. Doubly curved shell and coordinate system

The non-linear strain-displacement relations based on Sanders's shell theory can be expressed as:

$$\varepsilon_x = \varepsilon_x^o + \zeta\,\kappa_x \ ; \quad \varepsilon_y = \varepsilon_y^o + \zeta\,\kappa_y \ ; \ \gamma_{xy} = \gamma_{xy}^o + \zeta\,\kappa_{xy} \ ; \quad \gamma_{yz} = \gamma_{yz}^o \ ; \quad \gamma_{xz} = \gamma_{xz}^o \tag{1}$$

where $\varepsilon_j^0$ and $\kappa_j$ are defined as:

$$\varepsilon_x^o = \frac{1}{\alpha_1}\frac{\partial u_o}{\partial \xi_1} + \frac{w_o}{R_1} + \frac{1}{2\alpha_1^2}\left(\frac{\partial w_o}{\partial \xi_1}\right)^2 \ ; \quad \kappa_x = \frac{1}{\alpha_1}\frac{\partial \phi_1}{\partial \xi_1}; \ \varepsilon_y^o = \frac{1}{\alpha_2}\frac{\partial v_0}{\partial \xi_2} + \frac{w_0}{R_2} + \frac{1}{2\alpha_2^2}\left(\frac{\partial w_o}{\partial \xi_2}\right)^2 \ ; \kappa_y = \frac{1}{\alpha_2}\frac{\partial \phi_2}{\partial \xi_2}$$

$$\gamma_{xy}^o = \frac{1}{\alpha_1}\frac{\partial v_o}{\partial \xi_1} + \frac{1}{\alpha_2}\frac{\partial u_o}{\partial \xi_2} + \frac{1}{2\alpha_1\alpha_2}\frac{\partial w_o}{\partial \xi_1}\frac{\partial w_o}{\partial \xi_2} \quad ; \quad \gamma_{yz}^o = \frac{1}{\alpha_2}\frac{\partial w_o}{\partial \xi_2} + \phi_2 - \frac{v_o}{R_2} \tag{2}$$

$$\gamma_{xz}^o = \frac{1}{\alpha_1}\frac{\partial w_o}{\partial \xi_1} + \phi_1 - \frac{u_o}{R_1}; \ \kappa_{xy} = \frac{1}{\alpha_1}\frac{\partial \phi_2}{\partial \xi_1} + \frac{1}{\alpha_2}\frac{\partial \phi_1}{\partial \xi_2} - c_o\left(\frac{1}{\alpha_1}\frac{\partial v_o}{\partial \xi_1} - \frac{1}{\alpha_2}\frac{\partial u_o}{\partial \xi_2}\right)$$

$$c_0 = \frac{1}{2}\left(\frac{1}{R_1} - \frac{1}{R_2}\right); \ dx = \alpha_1 d\xi_1; \ dy = \alpha_2 d\xi_2$$

The stress-strain relation, accounting for thermal effects, in the shell coordinates for a $k^{\text{th}}$ layer can be expressed as:

$$\begin{Bmatrix}\sigma_x\\ \sigma_y\\ \tau_{xy}\\ \tau_{yz}\\ \tau_{xz}\end{Bmatrix}_k = \begin{bmatrix} Q_{11} & Q_{12} & Q_{16} & 0 & 0\\ Q_{12} & Q_{22} & Q_{26} & 0 & 0\\ Q_{16} & Q_{26} & Q_{66} & 0 & 0\\ 0 & 0 & 0 & Q_{44} & Q_{45}\\ 0 & 0 & 0 & Q_{45} & Q_{55}\end{bmatrix}_k \begin{Bmatrix}\varepsilon_x-\alpha_x T\\ \varepsilon_y-\alpha_y T\\ \gamma_{xy}-\alpha_{xy} T\\ \gamma_{yz}\\ \gamma_{xz}\end{Bmatrix}_k \tag{3}$$

where $Q_{ij}$ are the transformed elastic coefficients, $T$ is the given temperature distribution, $(\alpha_x, \alpha_y, \alpha_{xy})$ are the thermal expansion coefficients in the shell coordinates.

### 2.2 Sublaminate Model

The principal of sumlaminate (Figure 2) homogenization is based on the assumption that the in-plane strains and the interlaminar stresses through the thickness are constant [11-14]. The stress and strain vectors are then partitioned into two groups as [14]:

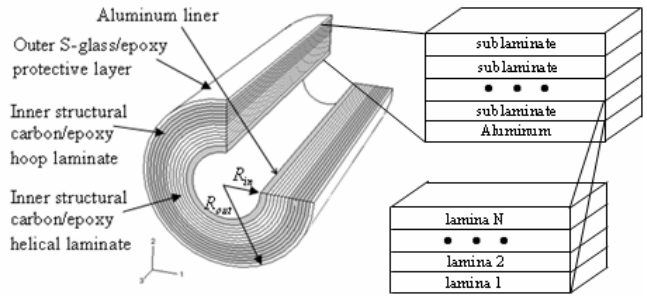


Figure 2. Structure scheme of hydrogen storage cylinder

$$\{\sigma\}=\begin{Bmatrix}\langle\sigma_o\rangle\\ \sigma_i\end{Bmatrix} \text{ where } \langle\sigma_o\rangle=\begin{Bmatrix}\langle\sigma_{zz}\rangle\\ \langle\sigma_{yz}\rangle\\ \langle\sigma_{xz}\rangle\end{Bmatrix} \quad \sigma_i=\begin{Bmatrix}\sigma_{xx}\\ \sigma_{yy}\\ \sigma_{xy}\end{Bmatrix}; \text{ and } \{\varepsilon\}=\begin{Bmatrix}\varepsilon_o\\ \langle\varepsilon_i\rangle\end{Bmatrix} \text{ where } \varepsilon_o=\begin{Bmatrix}\varepsilon_{zz}\\ \varepsilon_{yz}\\ \varepsilon_{xz}\end{Bmatrix} \quad \langle\varepsilon_i\rangle=\begin{Bmatrix}\langle\varepsilon_{xx}\rangle\\ \langle\varepsilon_{yy}\rangle\\ \langle\varepsilon_{xy}\rangle\end{Bmatrix} \tag{4}$$

where $\langle\ \rangle$ represents the term is constant through laminate.

The lamina stress-strain relationship in global coordinate can be written as:

$$\begin{Bmatrix}\langle\sigma_o\rangle\\ \sigma_i\end{Bmatrix}=\begin{bmatrix}C_{oo} & C_{oi}\\ C'_{oi} & C_{ii}\end{bmatrix}\begin{Bmatrix}\varepsilon_o\\ \langle\varepsilon_i\rangle\end{Bmatrix} \tag{5}$$

where $C_{oo}$, $C_{oi}$ and $C_{ii}$ are sub matrices of global stiffness matrix.

Partially inverting Eq. (5) yields

$$\begin{Bmatrix}\varepsilon_o\\ \sigma_i\end{Bmatrix}=\begin{bmatrix}C_{oo}^{-1} & -C_{oo}^{-1}C_{oi}\\ C'_{oi}C_{oo}^{-1} & -C'_{oi}C_{oo}^{-1}C_{oi}+C_{ii}\end{bmatrix}\begin{Bmatrix}\langle\sigma_o\rangle\\ \langle\varepsilon_i\rangle\end{Bmatrix} \tag{6}$$

After averaging, Eq. (6) can be expressed as

$$\begin{Bmatrix} \langle \varepsilon_o \rangle \\ \langle \sigma_i \rangle \end{Bmatrix} = \begin{bmatrix} A & -B \\ B^T & D \end{bmatrix} \begin{Bmatrix} \langle \sigma_o \rangle \\ \langle \varepsilon_i \rangle \end{Bmatrix} \tag{7}$$

where $A = \sum_{k=1}^{N} \frac{t_k}{t} \left( C_{oo}^{-1} \right)_k$, $B = \sum_{k=1}^{N} \frac{t_k}{t} \left( C_{oo}^{-1} C_{oi} \right)_k$, $D = \sum_{k=1}^{N} \frac{t_k}{t} \left( -C_{oi}' C_{oo}^{-1} C_{oi} + C_{ii} \right)_k$, $t_k$ is the thickness of each lamina in the smeared sublaminate and $t$ is the total thickness of the smeared sublaminate.

Partially inverting Eq. (7) yields the equivalent stiffness matrix $Q_{eq}$ of the sublaminate as

$$\begin{Bmatrix} \langle \sigma_o \rangle \\ \langle \sigma_i \rangle \end{Bmatrix} = \begin{bmatrix} A^{-1} & A^{-1}B \\ B^T A^{-1} & B^T A^{-1} B + D \end{bmatrix} \begin{Bmatrix} \langle \varepsilon_o \rangle \\ \langle \varepsilon_i \rangle \end{Bmatrix} = \begin{bmatrix} Q_{eq} \end{bmatrix} \begin{Bmatrix} \langle \varepsilon_o \rangle \\ \langle \varepsilon_i \rangle \end{Bmatrix} \tag{8}$$

The equivalent compliance matrix (for angle-ply laminate) is given by

$$S_{ij} = \begin{bmatrix} Q_{eq} \end{bmatrix}^{-1} \tag{9}$$

Equivalent engineering properties used for the simulation can be obtained from Eq. (9).

**2.3 Finite Element Model**

The generalized displacements in any element are given by

$$\{u, v, w, \phi_1, \phi_2\}^T = \sum_{i=1}^{N} \{u, v, w, \phi_1, \phi_2\}_i^T \psi_i \tag{10}$$

where N is the number of nodes in the element and $\psi_i$ are the interpolation functions.

The finite element equation for transient analysis can be written

$$\begin{bmatrix} M^e \end{bmatrix} \begin{Bmatrix} \ddot{\Delta}^e \end{Bmatrix} + \begin{bmatrix} K^e \end{bmatrix} \begin{Bmatrix} \Delta^e \end{Bmatrix} = \begin{Bmatrix} F^e \end{Bmatrix} + \begin{Bmatrix} F_T^e \end{Bmatrix} \tag{11}$$

where $\begin{bmatrix} M^e \end{bmatrix}$ is the elemental mass matrix, $\begin{bmatrix} K^e \end{bmatrix}$ is the elemental stiffness matrix, $\begin{Bmatrix} \Delta^e \end{Bmatrix}$ is the primary variables, $\begin{Bmatrix} F^e \end{Bmatrix}$ is the mechanical load vector and $\begin{Bmatrix} F_T^e \end{Bmatrix}$ is the thermal load vector.

The heat conduction equation can be expressed as

$$[C_T]\{\dot{T}\} + [K_T]\{T\} = \{H_T\} \tag{12}$$

where $[C_T] = \int_V \rho c N^n N^m dV$, $[K_T] = \int_V N^n \cdot \underline{k} \cdot N^m dV$, $[H_T] = \int_S N^n \cdot q dS$. $N^n$ (or $N^m$) are interpolation functions, $\rho$ is density, $\underline{k}$ is thermal conductivity, $c$ is specific heat, $q$ is surface heat flux and $T$ is temperature.

Combining Eq. (11) and (12), the sequentially coupled thermal-stress equation can be written as

$$\begin{bmatrix} M & 0 \\ 0 & 0 \end{bmatrix}^e \begin{Bmatrix} \{\ddot{\Delta}\} \\ 0 \end{Bmatrix}^e + \begin{bmatrix} 0 & 0 \\ 0 & C_T \end{bmatrix}^e \begin{Bmatrix} \{\dot{\Delta}\} \\ \{\dot{T}\} \end{Bmatrix}^e + \begin{bmatrix} K & 0 \\ 0 & K_T \end{bmatrix}^e \begin{Bmatrix} \{\Delta\} \\ \{T\} \end{Bmatrix}^e = \begin{Bmatrix} \{F\} + \{F_T\} \\ \{H_T\} \end{Bmatrix}^e \tag{13}$$

### 2.4 Failure Model

As the composite wall of the hydrogen cylinder experiences combined mechanical and transient thermal loads, a variety of failure types would occur in the process. A progressive failure model is employed in this study to identify the failure types based on failure criterion and predict the safety state of the cylinder. Hashin's failure criterion [15], accounting for four possible modes of ply failure, is used for this purpose.

1. Matrix tensile or shear cracking ( $\sigma_{22} + \sigma_{33} \geq 0$ ):

$$I_{mt} = \frac{\left(\sigma_{22} + \sigma_{33}\right)^2}{\left(F_T^t\right)^2} + \frac{\sigma_{12}^2 + \sigma_{13}^2 + \sigma_{23}^2 - \sigma_{22}\sigma_{33}}{\left(F_{LT}^S\right)^2} \tag{14}$$

2. Matrix compressive or shear cracking ( $\sigma_{22} + \sigma_{33} < 0$ )

$$I_{mc} = \frac{1}{F_T^c}\left[\left(\frac{F_T^c}{2\left(F_{LT}^S\right)}\right)^2 - 1\right]\left(\sigma_{22} + \sigma_{33}\right) + \frac{\left(\sigma_{22} + \sigma_{33}\right)^2}{4\left(F_{LT}^S\right)^2} + \frac{\sigma_{12}^2 + \sigma_{13}^2 + \sigma_{23}^2 - \sigma_{22}\sigma_{33}}{\left(F_{LT}^S\right)^2} \tag{15}$$

3. Fiber tensile fracture ( $\sigma_{11} \geq 0$ ): $I_{ft} = \left(\frac{\sigma_{11}}{F_L^t}\right)^2 + \frac{1}{\left(F_{LT}^S\right)^2}\left(\sigma_{12}^2 + \sigma_{13}^2\right)$ (16)

4. Fiber compressive fracture ( $\sigma_{11} < 0$ ): $I_{fc} = -\left(\frac{\sigma_{11}}{F_L^c}\right)$ (17)

where $F_L^t$, $F_L^c$, $F_T^t$, $F_T^c$ and $F_{LT}^S$ are longitudinal tensile strength, longitudinal compressive strength, transverse tensile strength, transverse compressive strength and shear strength of unidirectional ply respectively.

Once a specific type of failure is identified in the laminate, the reduction in its load-carrying capacity is accounted for by a reduction in its elastic moduli based on Tan's [16] assumption. The following material degradation rules are used for the analysis.

1. Matrix tensile or shear cracking: $E_2^d = D_2^T E_2$, $G_{12}^d = D_4^T G_{12}$ and $G_{23}^d = D_4^T G_{23}$, $D_2^T = D_4^T = 0.2$ (18)

2. Matrix compressive or shear cracking: $E_2^d = D_2^c E_2$, $G_{12}^d = D_4^c G_{12}$ and $G_{23}^d = D_4^c G_{23}$, $D_2^c = D_4^c = 0.4$ (19)

3. Fiber tensile fracture: $E_1^d = D_1^T E_1$, $D_1^T = 0.07$ (20)

4. Fiber compressive fracture: $E_1^d = D_1^c E_1$, $D_1^c = 0.14$ (21)

All the values of the internal state variables are obtained from literature [17].

### 2.5 Material Model

Mechanical and thermal properties of fiber reinforced composites vary significantly with temperature. As the carbon/epoxy laminate carries the pressure loading from the hydrogen gas, the effect of temperature on its material properties can not be ignored. However, the full required data of temperature dependent properties are not available in literature. Assumptions and curve fittings are necessary to obtain the material property data based on limited experimental data that is available. Numerous studies have been done on the curve fitting of temperature dependent properties. Gibson et al. [18] shows that a hyperbolic tan (tanh) function is capable of giving excellent fit to experimental data of material moduli and strength. The equation can be expressed as

$$\mathrm{P(T)} = \left[ \frac{P_U + P_R}{2} - \frac{P_U - P_R}{2} \tanh\left( k\left( T - T_g \right) \right) \right] \cdot C \tag{22}$$

where P(T) is temperature dependent material property, $P_U$ is the unrelaxed (low temperature) value of that property, $P_R$ is the relaxed (high temperature) value of that property, $k$ is a constant describing the breath of the distribution, $T$ is temperature, $T_g$ is the mechanically determined glass transition temperature and $C$ is a constant.

Table 1. Longitudinal modulus and strength of carbon/epoxy

| Longitudinal direction | | $P_U$ | $P_R$ | K | C | Tg ($^o$C) |
|---|---|---|---|---|---|---|
| Modulus (GPa) | | 133.35 | 111 | 0.0064 | 1 | 100 |
| Strength (MPa) | Tensile | 133.35 | 111 | 0.0064 | 1070/127 | 100 |
| | Compress. | 133.35 | 10.7 | 0.0150 | 1070/127 | 100 |

Table 2. Transverse modulus and strength of carbon/epoxy

| Transverse direction | | $P_U$ | $P_R$ | K | C | Tg ($^o$C) |
|---|---|---|---|---|---|---|
| Modulus (Gpa) | | 9.135 | 0.1 | 0.022 | 1 | 100 |
| Strength (MPa) | Tensile | 9.135 | 0.1 | 0.022 | 40/8.7 | 100 |
| | Compress. | 9.135 | 0.1 | 0.022 | 170/8.7 | 100 |

Table 3. Shear modulus and strength of carbon/epoxy

| Shear properties | $P_U$ | $P_R$ | K | C | Tg ($^o$C) |
|---|---|---|---|---|---|
| Modulus (GPa) | 4.515 | 0.045 | 0.02 | 1 | 100 |
| Strength(MPa) | 4.515 | 0.045 | 0.02 | 70/4.3 | 100 |

The experimental data of carbon/epoxy are taken from literature [19, 20]. Moduli are fitted using Eq. (22). The curves fitting parameters are listed in Tables 1-3. Moreover, $G_{13}$ is taken as the same value as $G_{12}$ and $G_{23} = E_2/2(1+\upsilon_{23})$. It has been assumed that the temperature variation of the ultimate longitudinal, transverse and shear strengths of carbon/epoxy follow the same pattern as that as the longitudinal, transverse and shear moduli respectively.

Table 4. Thermal expansion coefficients of carbon/epoxy

| | Experimental data | | | | | | | Extended data |
|---|---|---|---|---|---|---|---|---|
| Temperature ($^oC$) | 20 | 40 | 60 | 80 | 100 | 120 | 140 | 350 |
| $CTE_1(1\times10^{-6}/^oC)$ | 1.47 | 0.97 | 0.77 | 0.81 | 1.09 | 1.61 | 2.37 | 9.03 |
| $CTE_2(1\times10^{-6}/^oC)$ | 29.2 | 29.5 | 33.2 | 40.0 | 50.2 | 63.6 | 80.4 | 238.0 |

Table 5. Thermal properties for carbon/epoxy

| | Experimental data | | | | | | Extended data | |
|---|---|---|---|---|---|---|---|---|
| $T(^oC)$ | 0 | 20 | 70 | 95 | 120 | 170 | 260 | 350 |
| $Cp(kJ/kg/^oC)$ | 0.8 | 0.86 | 1.08 | 1.28 | 1.4 | 1.5 | 1.67 | 1.84 |
| Longitudinal Thermal conductivity | | | Transverse Thermal conductivity | | | | | |
| $K_{11}$ = 6.5 W/m/$^o$C | | | $K_{22}$ = 0.65 W/m/$^o$C | | | $K_{33}$= 0.65 W/m/$^o$C | | |

Table 6. Mechanical properties of S-glass/epoxy

| $E_1$ (GPa) | $E_2$ (GPa) | $G_{12} = G_{13}$ (GPa) | $G_{23}$ (GPa) | $\upsilon_{12}$ | $\alpha_1$ (1/°C) | $\alpha_2$ (1/°C) |
|---|---|---|---|---|---|---|
| 55 | 16 | 7.6 | 5.0 | 0.28 | $6.3\times10^{-6}$ | $32\times10^{-6}$ |
| Strengths | $F_L^t$ | $F_L^c$ | $F_T^t$ | $F_T^c$ | $F_{LT}^S$ | |
| MPa | 1620 | 690 | 40 | 140 | 60 | |

Table 7. Mechanical and thermal properties of aluminum 6061-T6

| Elastic Modulus, E | Poisson's ratio, $\upsilon$ | Yield strength, $\sigma_y$ | $\alpha$ (1/°C) |
|---|---|---|---|
| 70 GPa | 0.33 | 455 MPa | $24.3\times10^{-6}$ |
| Density | Heat capacity | Heat conductivity | |
| 2700 kg/m$^3$ | 1000 J/g·K | 250 W/m·K | |

The thermal properties of carbon/epoxy are listed in Tables 4 and 5. As thermal conductivity and specific heat of glass/epoxy are very close to those of carbon/epoxy, the same values are taken for glass/epoxy. The other material properties for glass/epoxy are listed in Table 6. Properties of innermost aluminum liner are listed in Table 7.

## 3.0 RESULTS AND DISCUSSION

The sublaminate model, failure model and the material model are incorporated in the finite element model using user subroutine to predict the response of hydrogen storage tanks subjected to combined mechanical and transient thermal loads. Results are presented for a cylinder diameter of 0.44 m (17 inches). The composite cylinder consists of inner aluminum liner, six sublaminates of carbon/epoxy and one outer protection sublaminate of glass/epoxy. Each sublaminate consists of four lamina (see Figure 3). The aluminum liner is 2.54 mm thick. Each of the hoop sublaminate has a total thickness of 5.875 mm and

each of the helical sublaminate has a total thickness of 3.525 mm. The glass/epoxy sublaminate has a thickness of 4 mm.

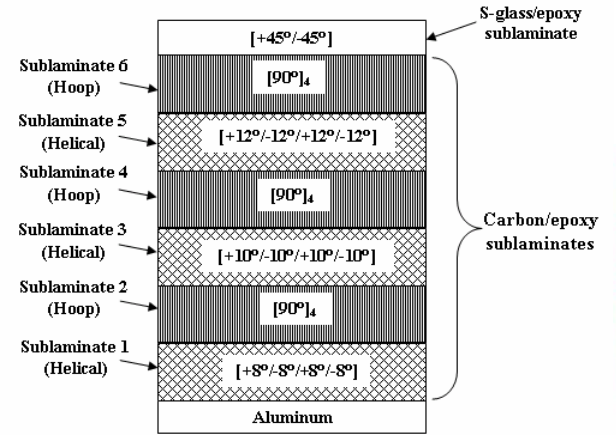


Figure 3. Sublaminate stacking sequence

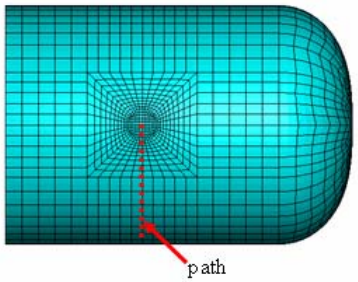


Figure 4. Finite element model of hydrogen storage cylinder

A constant heat source of 75,000 Watt/m$^2$ acts over a circular region of 30 mm radius through out the analysis. The cylinder is also subjected to an internal pressure of 34.5 MPa. The composite shell uses the S8RT element which is based on a doubly curved shell element accounting for transverse shear deformation and heat transfer. The finite element model is built and meshed using ABAQUS commercial finite element code (see Figure 4). The transient analysis is carried out for 120 seconds.

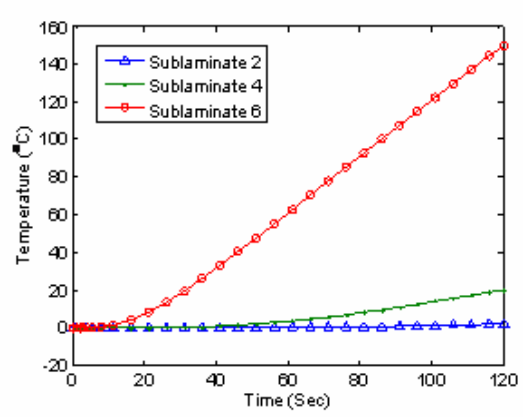


Figure 5. Temperature variation with time at center of heat source for various sublaminates

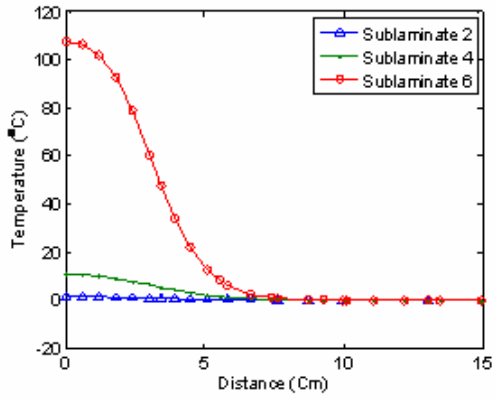


Figure 6. Temperature distribution along path (see Figure 4) at t = 90 s for various sublaminates

Figure 5 shows the temperature variation at the center of the heat source with time for sublaminates 2, 4 and 6. The temperature of the sublaminate closest to the heat source (sublaminate 6) increases rapidly with time while the temperature increase in the inner sublaminates is at a much slower rate. Figure 6 shows the temperature profile along the selected path shown in Figure 4 after 90 seconds. It can be observed that the temperature close to the heat sources is high and as the distance from the heat source increases, the temperature drops rapidly. This can be attributed to the low thermal conductivity of carbon/epoxy. It can also be noted that the temperature drops drastically through the thickness of the laminates. Even after 120 seconds, the highest temperature in the carbon/epoxy sublaminates is 160°C. This can be attributed to glass/epoxy sublaminate protecting the carbon/epoxy sublaminates.

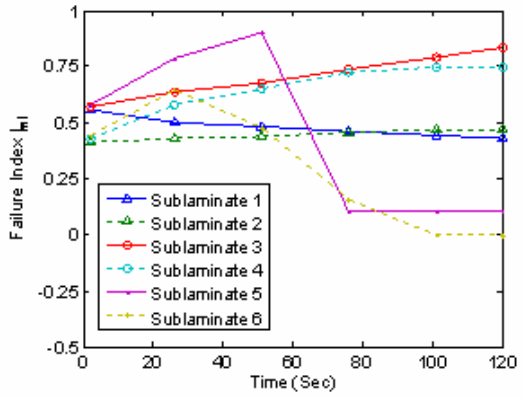


Figure 7. Matrix tensile/shear cracking failure index $I_{mt}$ as a function of time

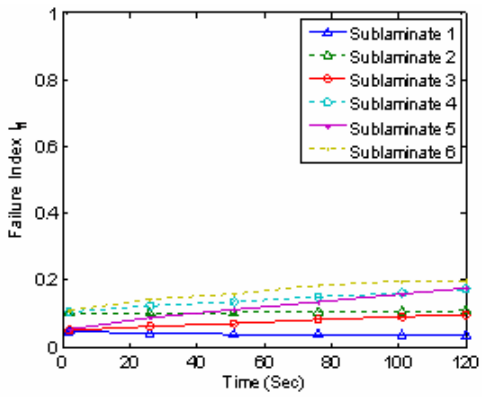


Figure 8. Fiber tensile failure index $I_{ft}$ as a function of time

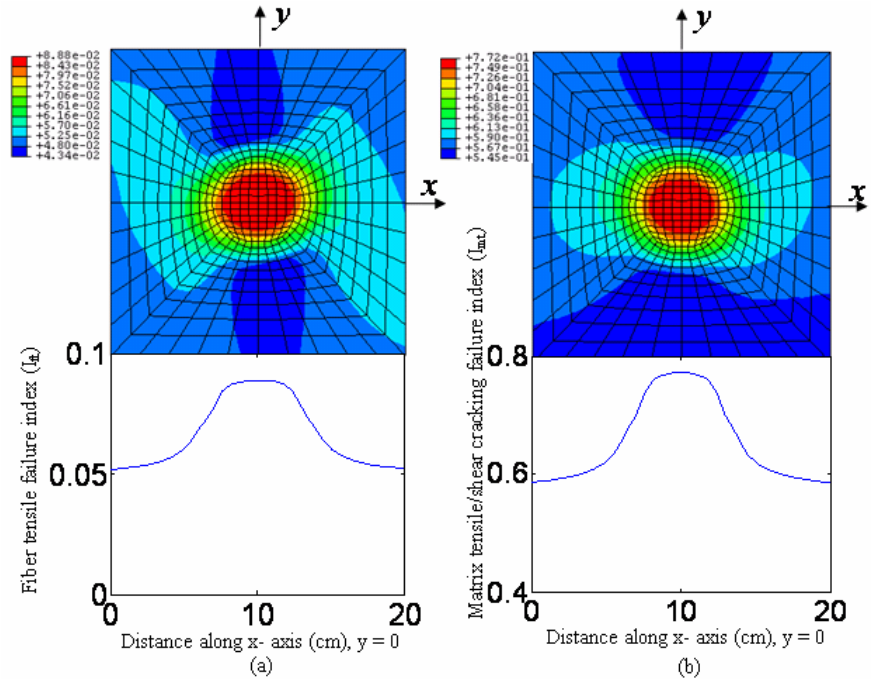


Figure 9. Counter of (a) fiber tensile failure index $I_{ft}$ and (b) matrix tensile/shear cracking failure index $I_{mt}$ around heat source ( sublaminate 3, t = 90 s)

Figure 7 shows the variation of matrix failure index ($I_{mt}$) as a function of time for sublaminates 1 through 6. It can be observed that the matrix failure index for the inner sublaminates (sublaminates 1 and 2) does not vary much as they are away from the heat source. For the intermediate sublaminates (sublaminates 3 and 4), the matrix failure index increases with time (temperature also increases with time). For the outer most sublaminates (sublaminates 5 and 6), the matrix failure index initially increases and then drops. The matrix failure index for sublaminate 6 drops first (after 30 Sec) followed by sublaminate 5 (after 50 sec). This can be explained due to the large thermal strain caused by the higher temperature in sublaminate 6. It should be noted that the thermal expansion coefficient in the transverse direction increases rapidly with an increase in temperature. As a result the thermal strain in the outermost sublaminate (sublaminate 6) is much higher causing it to relax the mechanical loading thus resulting in a drop in the matrix failure index.

Figure 8 plots the variation of fiber failure index ($I_{fi}$) as a function of time for sublaminates 1 through 6. It can be observed that the fiber failure index of the outermost sublaminate (sublaminates 5 and 6) slightly increases with time while fiber failure index of the inner sublaminates (sublaminates 1 and 2) is almost constant. The increase in the failure index of the outer layers can be attributed to the thermal loading. It should be noted that the maximum failure index if the fibers is < 0.2 indicating that overall failure of the tank will be caused due to the failure of the matrix material.

Figure 9 shows the contour plots of the fiber and the matrix failure indices after 90 seconds in sublaminate 3. The variation of the fiber and matrix failure indices along the x – axis at y = 0 is also plotted in the Figure 9. It can be noted that the failure index is highest in the region subjected to the transient heat source. Also, the failure index distribution throughout the sublaminate is not uniform. In the fiber failure index contour plot, the tilt in the angle can be attributed to the orientation of the fibers in the lamina.

## 4.0 CONCLUSIONS

A finite element model has been developed to analyze composite hydrogen storage cylinders subjected to transient localized thermal loads and internal pressure. A doubly shell has been used to model the hydrogen cylinder. A sublaminate model has been developed and implemented in ABAQUS to reduce computational time. A temperature dependent material model and failure model have been developed and implemented in ABAQUS using user subroutine to accurately predict various types of failure for the hydrogen storage cylinder. The developed model can be used to accommodate various types of thermal and mechanical loading, lamina stacking sequence and lamina thickness to establish safe working conditions and design limits for hydrogen storage cylinders.

## ACKNOWLEDGEMENTS

The project is sponsored by the US. Department of Transportation and University Transportation Center.

## REFERENCES

1. Knapp, R. H., Shimabukuro, T. A. and Robertson, I. N., Fiber Optic Sensor System (FOSS) for Filament-Wound Gas Cylinders, Proceeding of the Eleventh International Offshore and Polar Engineering Conference, Stavanger, Norway, June 17-22, 2001, pp. 191-196.
2. Parnas, L. and Katirci, N., Design of Fiber-reinforced Composite Pressure Vessels under Various Loading Conditions, Composite Structures, **58**, 2002, pp. 83–95.
3. Akcay, I. H. and Kaynak, I., Analysis of Multilayered Composite Cylinders under Thermal Loading, Journal of Reinforced Plastics and Composites, **24**, 2005, pp.1169-1179.
4. Sayman, O., Analysis of Multi-layered Composite Cylinders under Hygrothermal Loading, Composites: Part A, **36**, 2005, pp. 923–933.
5. Yee, K. C. and Moon, T. J., Plane Thermal Stress Analysis of an Orthotropic Cylinder Subjected to an Arbitrary Transient Asymmetric Temperature Distribution, Transactions of the ASME, **69**, September 2002, pp. 632-640.
6. Lee, Z. Y., Chen, C. K. and Hung, C. I., Transient Thermal Stress Analysis of Multilayered Hollow Cylinder, ACTA Mechanica, **151,** 2001, pp. 75-88.

7. Lu, X., Tervola, P. and Viljanen, M., Transient Analytical Solution to Heat Conduction in Multi-dimensional Composite Cylinder Slab, International Journal of Heat and Mass Transfer, **49**, 2006, pp. 1107-1114.
8. Jacquemin, F. and Vautri, A., Analytical Calculation of the Transient Thermoelastic Stresses in Thick Walled Composite Pipes, Journal of Composite Materials, **38**, 2004, pp. 1733-1751.
9. Chandrashekhara, K. and Bhimaraddi, A., Thermal Stress Analysis of Laminated Doubly Curved Shells using a Shear Flexible Finite Element, Computers and Structures, **52**, 1994, pp. 1023-1030.
10. Chandrashekhara, K. and Schroeder, T., Nonlinear Impact Analysis of Laminated Cylindrical and Doubly Curved Shells, Journal of Composite Materials, **29**, 1995, pp. 2160-2179.
11. Chou, P. C. and Carleone, J., Elastic Constants of Layered Media, Journal of Composite Materials, **6**, 1972, pp. 80-93.
12. Sun, C. T. and Li, S., Three-Dimensional Effective Elastic Constants for Thick Laminates, Journal of Composite Materials, **22**, 1988, pp. 629-639.
13. Chen, H. and Tsai, S. W., Three-Dimensional Effective Moduli of Symmetric Laminates, Journal of Composite Materials, **30**, 1996, pp. 906-916.
14. Whitcomb, J. and Noh, J., Concise Derivation of Formulas for 3D Sublaminate Homogenization, Journal of Composite Materials, **34**, 2000, pp. 522-535.
15. Hashin, Z., Failure Criteria for Unidirectional Fiber Composites, Journal of Applied Mechanics, **47**, 1980, pp. 329-334.
16. Tan, S. C., A Progressive Failure Model for Composite Laminates Containing Openings, Journal Composite Materials, **25**, 1991, pp. 556-577.
17. Camanho, P. P. and Matthews, F. L., A Progressive Damage Model for Mechanically Fastened Joints in Composite Laminates, Journal of Composite Materials, **33**, 1999, pp. 2248-2278.
18. Gibson, A. G., Wu, Y. S., Evans, J. T. and Mouritz, A. P., Laminate Theory Analysis of Composites Under Load in Fire, Journal of Composite Materials, **40**, 2006, pp. 639-658.
19. Yoon, K. J. and Kim, J., Prediction of Thermal Expansion Properties of Carbon/Epoxy Laminates for Temperature Variation, Journal of Composite Materials, **34**, 2000, pp. 90-100.
20. Kalogiannakis, G., Hemelrijck, D. V. and Assche, G. V., Measurements of Thermal Properties of Carbon/Epoxy and Glass/Epoxy using Modulated Temperature Differential Scanning Calorimetry, Journal of Composite Materials, **38**, 2004, pp. 163-175.